PCCP

PAPER

View Article Online
View Journal | View Issue

Cite this: *Phys. Chem. Chem. Phys.*, 2015, **17**, 31769

Understanding the fundamentals of redox mediators in Li–O_2 batteries: a case study on nitroxides†

Benjamin J. Bergner,[a] Christine Hofmann,[b] Adrian Schürmann,[a] Daniel Schröder,[a] Klaus Peppler,[a] Peter R. Schreiner[b] and Jürgen Janek*[a]

Received 30th July 2015,
Accepted 26th October 2015

DOI: 10.1039/c5cp04505c

www.rsc.org/pccp

The development of aprotic lithium–oxygen (Li–O_2) batteries suffers from high charging overvoltages. Dissolved redox mediators, like nitroxides, providing increased energy efficiency and longer lifetime are promising tools to overcome this challenge. Since this auspicious concept is still in its infancy, the underlying chemical reactions as well as the impact of the different (electro)chemical parameters are poorly understood. Herein, we derive an electrochemical model for the charging reactions, which is validated by potentiostatic measurements. The model elucidates the impact of the major factors including basic cell parameters and the chemical properties of the redox mediator. The model is applied to the promising class of nitroxides, which is systematically investigated by using derivatives of TEMPO (2,2,6,6-tetramethyl-1-piperidinyloxy), AZADO (2-azaadamantane-*N*-oxyl), and an azaphenalene based nitroxide. The nitroxides are electrochemically characterized by cyclic voltammetry and their performance as redox mediators is studied in Li–O_2 batteries with an ether-based electrolyte. Based on the presented model, the charging profiles of the different nitroxide redox mediators are correlated with their molecular structures.

1. Introduction

Since their introduction in 1996 by Abraham and Jiang, aprotic lithium–oxygen (Li–O_2) batteries have emerged as viable post-lithium-ion battery systems owing to their exceptionally high specific energy density, that theoretically reaches up to 11 400 W h kg^{-1} for the charged state.[1] Cycling of aprotic Li–O_2 batteries involves formation and decomposition of insoluble and poorly electronically conducting lithium peroxide (Li_2O_2), which causes severe overvoltages, depending on the morphology of the Li_2O_2 discharge product.[2–4] Degradation of the electrolyte and the carbon cathode in the reactive electrochemical environment and the presence of different dioxygen species (O_2, O_2^-,O_2^{2-}) represents an additional challenge.[5,6] Hence, current Li–O_2 cells are still faced with severe limitations including poor cycle life and high overvoltages – especially during charging.[7] The origin of the high and mostly continuously increasing charging voltages is still a subject of controversial discussions.[1] Either the poor bulk-conductivity of Li_2O_2 itself[8] or the additional accumulation of degradation products[6] are assumed as the major factors. Interestingly, the charging kinetics of Na–O_2 cells proceeds *via* a completely different route with very small overvoltages, as the superoxide NaO_2 rather than the peroxide forms.[9,10] A promising strategy to reduce the comparable high charging overvoltages is the use of a dissolved redox mediator (RM), which acts as a mobile charge carrier within the liquid electrolyte.[11,12] Herein, the charging voltage is directly connected to the redox potential of the mediator, and a second reaction path opens. Thus charging is no longer determined exclusively by the complex and slow processes within the solid reaction product.

Various molecular compounds have been proposed as possible redox mediators including TTF (tetrathiafulvalene),[13] LiI,[13,14] $LiNO_3$[15] and various metal complexes.[16–18] Previously we have shown that even small concentrations of the nitroxide TEMPO (2,2,6,6-tetramethyl-1-piperidinyloxy) provide lasting reduction of the charging overvoltages in Li–O_2 cells.[19] Typically, Li–O_2 cells with redox mediators exhibit longer life times than similar cells without additives.[16,19,20] This is mainly ascribed to a reduced impact of degradation reactions, which mostly occur at high potentials.[21] Recent studies indicate, that several redox mediators also contribute to discharge processes affecting, for instance, the maximal discharge capacity[16,19] or the role of decomposition reactions.[14]

[a] *Institute for Physical Chemistry, Justus-Liebig University Giessen, Heinrich-Buff-Ring 17, 35392 Giessen, Germany. E-mail: Juergen.Janek@phys.Chemie.uni-giessen.de*
[b] *Institute of Organic Chemistry, Justus-Liebig University Giessen, Heinrich-Buff-Ring 17, 35392 Giessen, Germany*

† Electronic supplementary information (ESI) available. See DOI: 10.1039/c5cp04505c

Although the basic characteristics of Li–O_2 cells with redox mediators were profoundly investigated previously,[13,19,20] further development still suffers from an insufficient understanding of the electrochemical processes. The major factors controlling the mediated charge transfer are still unknown, since an appropriate electrochemical model is missing. Possible control parameters range from the basic cell parameters to the chemical structure of the redox mediator itself. As all investigated redox mediators are chemically quite different,[13,16,19,20] the relation between the chemical structure of the mediator and its electrochemical performance in a Li–O_2 battery is still unknown. A systematic approach requires chemically closely related compounds, as successfully illustrated by Matsuda *et al.* for various transition metal complexes with macrocyclic ligands.[17]

Systematically studying the chemical group of nitroxides, this work combines electrochemical and chemical concepts to understand the fundamentals of redox mediators in Li–O_2 cells. Primarily, a one-dimensional electrochemical model is derived to describe the charge transfer by the redox mediator. Subsequently, we transfer the underlying concept to an appropriate model system. Herein, potentiostatic measurements with a geometrically well-defined LFP/C(O_2) cell are used to evaluate the electrochemical model. Finally, selected nitroxide compounds are investigated as redox mediators under typical conditions of Li–O_2 batteries to evaluate the impact of their chemical structure.

2. Experimental and methods

2.1 Materials

2.1.1 General aspects. TEMPO (2,2,6,6-tetramethyl-1-piperidinyloxy, 99%), 4-methoxy-TEMPO (4-methoxy-2,2,6,6-tetramethyl-1-piperidinyloxy, 99%), AZADO (2-azaadamantane-*N*-oxyl, 96%), 1-Me-AZADO (1-methyl-2-azaadamantane-*N*-oxyl, 97%), 2,2,5-trimethyl-4-phenyl-3-azahexane-3-nitroxide, *tert*-amy-*tert*-butyl-nitroxide (95%), LiTFSI (lithium bistrifluoro-methane-sulfonimidate, 99.95%) and diglyme (2-methoxyethyl ether, 99.5%) were purchased from Sigma Aldrich. TMAO (1,1,3,3,-tetramethyl-2,3-dihydro-2-azaphenalene-2-yloxyl) was synthesized as described in Section 2.1.2. The chemical structures of the applied nitroxides are illustrated in Scheme 2. Lithium (99.9%) was ordered from Rockwood Lithium. TEMPO and 4-methoxy-TEMPO were purified by sublimation. AZADO and 1-Me-AZADO were purified electrochemically by several initial CV cycles to mitigate an additional oxidation peak at about 3.54 V. The corresponding reduction peaks of the investigated nitroxides remained fully unchanged during the procedure. Diglyme was distilled and subsequently dried over activated molecular sieves (3 Å) for two months to finally achieve a water content of <2.0 ppm (determined by Karl–Fischer titration). LiTFSI was vacuum-dried for 16 h at 160 °C in a Büchi oven prior to use. All electrolytes were prepared and stored in an argon filled glovebox.

2.1.2 Synthesis of TMAO. TMAO was synthesized from 1,8-naphthalic anhydride in four steps as described in the literature.[22] Analytical data of the isolated product were identical with those reported in the literature.[22]

2.2 Potentiostatic measurements

2.2.1 General aspects. The potentiostatic measurements were conducted with "cell 1" using a Swagelok® design. The setup of cell 1 is illustrated in Fig. 1 and contained a delithiated lithium iron phosphate (LFP) counter electrode with ∅ = 12 mm (comprising of 84 wt% LFP, 8 wt% polyvinylidene fluoride, 4 wt% carbon black, 4 wt% graphite), a lithium reference electrode, a polished glassy carbon (GC) working electrode with ∅ = 12 mm (HTW Hochtemperatur Werkstoffe GmbH) and two stainless steel current collectors. The redox state of the LFP electrode was individually selected so that the LFP electrode was able to fully oxidize the initial amount of dissolved TEMPO in the corresponding experiment. Working electrode and counter electrode were separated by a glass fibre separator with ∅ = 8 mm (Whatman, GF/A) providing an additional rectangular connection to the reference electrode. The separator was surrounded by a PTFE ring with outer ∅ = 12 mm, inner ∅ = 8 mm and a thickness of 200 μm ensuring a defined distance between both electrodes. Each time, 25 μL freshly prepared electrolyte were used comprising of 1 M LiTFSI/diglyme with TEMPO in concentrations up to 200 mM. In case of the distant-dependent measurements, additional layers of separator soaked with 15 μL electrolyte and surrounded by a PTFE ring were stacked atop of the initial layer. The duration of the potentiostatic measurements was intentionally selected so that on average each TEMPO molecule is oxidized more than once, mostly even more than twice, at the GC electrode during re-charge. The experiments were performed with either a SP300 or VMP3 galvanostat/potentiostat (both BioLogic Science Instruments).

2.2.2 Porosity ε of the separator. The porosity ε_0 of the pristine separator with d = 260 μm was determined by mercury intrusion porosimetry as $\varepsilon_0 = 0.90 \pm 0.05$. The porosity ε of the compressed separator with d = 200 μm was calculated by:

$$\varepsilon = \frac{200 - 260(1 - \varepsilon_0)}{200} = 0.87 \pm 0.04$$

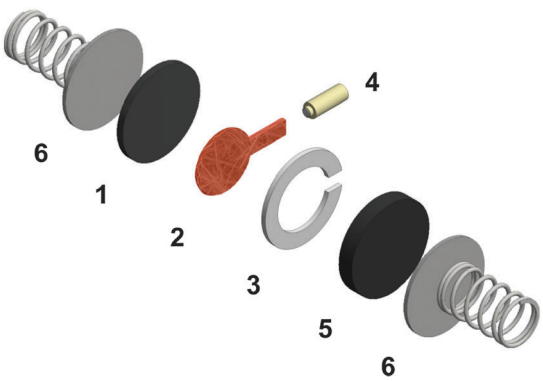

Fig. 1 Setup of "cell 1" comprising of a LFP counter electrode (1), a porous separator soaked with the typically red electrolytes (2), a PTFE spacer (3), a lithium reference electrode (4), a glassy carbon working electrode (5) and (6) stainless steel current collectors.

2.3 Cyclic voltammetry (CV)

Cyclic voltammetry measurements were conducted in a gas-tight glass cell which was equipped with two gas valves, a glassy carbon working electrode (BAS Inc., ∅ = 6 mm), an in-house built lithium reference electrode and a platinum wire as counter electrode (BAS Inc.). Typically, 4 mL of 1 M LiTFSI/diglyme were used as electrolyte which additionally contained 10 mM of the different nitroxides. Reference measurements were conducted with pure 1 M LiTFSI/diglyme. The cells were assembled in an argon filled glovebox. Primarily, scan rate dependent measurements were conducted within the glovebox using a SP300 galvanostat/ potentiostat (BioLogic). After purging the cells with pure oxygen (>99.999, Praxair), a second CV was recorded using a VMP3 galvanostat/potentiostat (BioLogic). All CVs were started at the open circuit potential (OCP), scanned to 2.0 V *vs.* Li^+/Li and subsequently to 4.55 V *vs.* Li^+/Li finally returning to the OCP.

2.4 Galvanostatic cycling of Li–O_2 cells

2.4.1 General aspects. Galvanostatic cycling was conducted in "cell 2" using a Swagelok® design which comprised three electrodes and a gas chamber (around 9 mL). The setup of "cell 2" is illustrated in Fig. 2. All Li–O_2 cells were assembled in an argon filled glovebox using a disc shaped lithium anode (∅ = 10 mm), a disc shaped porous separator (∅ = 12 mm, Whatman, GF/A) soaked with 60 μL electrolyte, a porous carbon cathode casted on another disc shaped separator (∅ = 10 mm) and two stainless steel current collectors. The potential of the carbon electrode was determined relative to a lithium reference electrode, which was laterally attached by using a small strap of separator (Whatman, GF/A). Most experiments were carried out with 1 M LiTFSI/diglyme as base electrolyte additionally containing 10 mM of the investigated nitroxides. Further measurements were conducted with pure 1 M LiTFSI/diglyme or with 100 mM TEMPO in 1 M LiTFSI/diglyme. The lithium anode was pretreated with 0.1 M LiTFSI/propylene carbonate for one week to improve SEI formation and subsequently washed with pure diglyme. After purging the gas chamber with pure oxygen (>99.999, Praxair) the cells were cycled using a battery cycler system 4300 from Maccor. The cells were discharged with a (geometric) current density of 0.1 mA cm^{-2} to a fixed capacity of 1000 mA h g_C^{-1} or to fixed cut-off voltage of 2.0 V and subsequently charged with the same current density to 4.2 V.

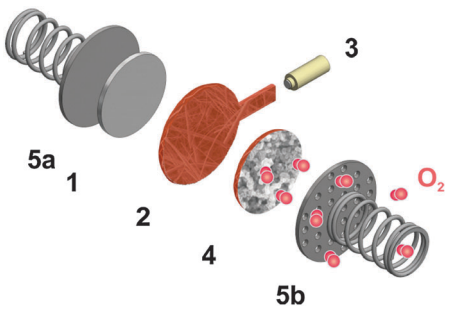

Fig. 2 Setup of "cell 2" comprising of a lithium anode (1), a porous separator soaked with the typically red electrolytes (2), a lithium reference electrode (3), a porous carbon cathode casted on an additional layer of separator (4) and stainless steel current collectors (5a & 5b). Oxygen is supplied from a closed gas vessel mounted atop of the current collector 5b.

2.4.2 Preparation of the porous cathodes. A slurry containing 23 mg of a PTFE dispersion (60 wt% in water, purchased from Sigma Aldrich) and 96 mg Ketjen Black (AkzoNobel) in 15 mL 2-propanol was cast on disc-shaped glass fibre separators and subsequently dried at 160 °C in a vacuum oven. The final carbon loading ranged from 0.4 to 0.8 mg cm^{-2}.

2.5 X-ray diffraction (XRD) analysis

X-ray diffraction data of fully discharged and charged carbon electrodes (cut-off voltages of 2.0 V and 4.2 V) were recorded with an Empyrean powder diffractometer (PANalytical) using a Cu K_α source (40 kV, 40 mA). The corresponding Li–O_2 cells were disassembled in a glovebox, the carbon electrodes were subsequently washed with pure diglyme and analysed in a gas-tight sample holder with a 7.5 μm thick Kapton foil (Chemplex) atop. The diffraction data were further processed with the software X'Pert Highscore Plus (PANalytical) including a baseline subtraction and a *z*-correction of the sample position.

3. Theoretical considerations

Modelling the charging processes

While the (electro)chemical reactions of regular Li–O_2 cells are complex and elusive in view of all possible (side) reactions,[1,8] a clear and simple reaction scheme was proposed for the charging of Li–O_2 cells with redox mediators, thereby assuming much less side reactions.[13,19] We surmise that the dissolved redox mediator RM is oxidized at electrochemically active parts of the carbon surface to form the cation RM^+ (eqn (1)), which diffuses to the electrically insulating Li_2O_2 particles. Li_2O_2 is then instantaneously oxidized and decomposed by RM^+ releasing molecular oxygen, lithium ions and the reduced species RM (eqn (2)).

$$RM \rightarrow RM^+ + e^- \quad (1)$$

$$RM^+ + \tfrac{1}{2}Li_2O_2 \rightarrow RM + Li^+ + \tfrac{1}{2}O_2 \quad (2)$$

RM subsequently diffuses back to the uncovered parts of the carbon electrode, where the next catalytic cycle is initiated. Hence, a continuous shuttle of RM and RM^+ arises between the carbon electrode and Li_2O_2. The diffusion paths of RM and RM^+ are essential factors for the charging processes in Li–O_2 with redox mediators but have not been discussed up now. We assume that the diffusion paths start at a small number of poorly covered or uncovered sites on the carbon cathode and lead to the directly adjacent Li_2O_2 particles or films. Since the closest Li_2O_2 particles are readily decomposed after a short charging period, the distance of the diffusion path is expected to rise with increasing charging depth. We do no assume that the uncovered area of the carbon surface increases during the charging step, even though the Li_2O_2 particles are continuously removed by RM^+. Rather, Li_2CO_3 is presumed to accumulate on the surface, which is not fully decomposed below 4.0 V *vs.* Li^+/Li.[21]

Initially Li_2CO_3 was formed by a direct reaction between the Li_2O_2 particles and the carbon surface.[6]

The charging step additionally includes the diffusion and reduction of Li^+ ions at the lithium electrode, which exhibits a significantly lower overpotential than the oxidation of Li_2O_2. Hence, the present model will solely consider the processes at the carbon electrode, which almost completely determine the charging profiles.

In order to derive an appropriate electrochemical description, the complex and inhomogeneous environment of the carbon electrode is simplified to a well-defined model system, compare Fig. 3. The model includes Li_2O_2 and an uncovered part of the carbon electrode, which are separated by the constant distance d. The space between Li_2O_2 and the carbon electrode is completely filled with the liquid electrolyte containing the dissolved redox mediator RM. Note that the model is restricted to the intermediate space between Li_2O_2 and the carbon electrode and therefore diffusion of the redox mediator from/into the bulk electrolyte is not considered. The diffusion of RM^+ into the bulk electrolyte will finally cause a detrimental shuttle to the lithium electrode competing with the desired shuttle to Li_2O_2. Unless otherwise stated, the term "shuttle" will hereafter solely refer to the catalytic shuttle to Li_2O_2. Neglecting the diffusion from/into the bulk electrolyte seems to be appropriate for the major part of the charging step, since we did not observe a significant diffusion to the anode under cycling conditions.[19] However, the final charging period is excluded, since depletion of Li_2O_2 is expected to promote the diffusion of RM^+ into the bulk electrolyte.

The following transport and reactions steps as well as boundary conditions and assumptions are taken into account in defining the model system:

Mass transport

• Most redox couples exhibit similar chemical structures in their oxidized and reduced forms, *e.g.*, $TEMPO^+$/TEMPO or TTF^+/TTF. According to the Marcus theory, the inner sphere and outer sphere reorganization energy of the electron transfer are low in this case leading to a minimal activation energy. Hence, charge transfer kinetics at the carbon electrode are significantly faster than the mass transport of the redox mediator by diffusion and can be neglected.[23] We will in particular consider RM couples with a distinctly higher redox potential than the standard potential for the formation of Li_2O_2 (E_0 = 2.96 V *vs.* Li^+/Li), *e.g.* TEMPO or TTF ($E_0 > 3.4$ V *vs.* Li^+/Li). Hence, the oxidized species RM^+ is instantaneously reduced at the Li_2O_2 surface leading to a fast charge transfer at this side as well.

• Typical electrolytes for Li–O_2 batteries provide high Li^+ concentrations and a high Li^+ conductivity, exceeding the conductivity contribution of the redox mediator in the applied concentration range. Hence, the mass transport of the redox mediator is a purely diffusion-driven process, while migration is mainly conducted by Li^+ ions.

• The diffusion coefficients D of RM and RM^+ are set equal, since similar chemical structures are assumed for RM and RM^+.

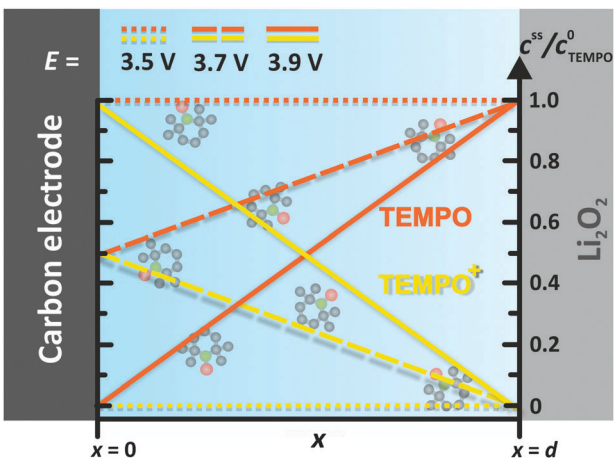

Fig. 3 TEMPO and $TEMPO^+$ concentration profiles between the carbon electrode and the Li_2O_2 surface at different electrode potentials E. Herein, E_0 = 3.70 V *vs.* Li^+/Li was used for the $TEMPO^+$/TEMPO redox couple, compare Table 1.

Steady state conditions

• The oxidation reaction at the electrode surface directly depletes the concentration of RM and leads to the formation of a diffusion layer. This layer gradually increases from the electrode surface into the bulk electrolyte.[23,24] The maximal thickness of the diffusion layer is limited by the Li_2O_2 surface, where RM^+ is directly reduced – thus to the distance d. Herein, stationary conditions successively establish stable concentration gradients for both species. A similar behaviour was already reported for the diffusion of redox shuttle additives in Li-ion batteries.[25]

• The stationary state is reached after $t \approx d^2/D$,[24,26] which corresponds to the mean time t for one RM molecule to diffuse the distance d from the carbon electrode to Li_2O_2. Estimating $d < 1$ μm on the basis of the Li_2O_2 particle size[27] and using $D > 1 \times 10^{-6}$ cm^2 s^{-1}, compare Table 2, stationary conditions are quickly established after $t < 1$ s. Since charging typically lasts for several hours, the short pre-stationary period will be ignored for the further considerations.

Surface concentration

• RM and RM^+ are assumed as chemically stable. Degradation reactions are neglected.

• Due to the assumption of equal diffusion coefficients for RM and RM^+, the total concentration of redox mediator molecules will remain unchanged within every infinitesimal volume element of the electrolyte along the cell coordinate x, see Fig. 3:

$$c^{ss}_{RM^+}(x) + c^{ss}_{RM}(x) = c^0_{RM}, \quad (3)$$

where c^0_{RM} is the initial concentration of the redox mediator RM and $c^{ss}_{RM^+}(x)$, $c^{ss}_{RM}(x)$ are the concentrations of RM^+ and RM at position x under steady state conditions.

• Assuming a higher redox potential of RM^+/RM than the standard potential for the formation of Li_2O_2, RM^+ is directly reduced at the Li_2O_2 surface ($x = d$):

$$c^{ss}_{RM^+}(d) = 0 \quad (4)$$

$$c^{ss}_{RM}(d) = c^0_{RM} \quad (5)$$

where $c^{ss}_{RM^+}(d)$, $c^{ss}_{RM}(d)$ are the concentrations of RM^+, RM at the Li_2O_2 surface under steady state conditions.

• Assuming steady state conditions, the concentrations of RM and RM^+ at the carbon electrode ($x = 0$) control the electrode potential by the Nernst equation:

$$E = E_0 + \frac{RT}{zF}\ln\frac{c^{ss}_{RM^+}(0)}{c^{ss}_{RM}(0)}, \quad (6)$$

where E is potential of the carbon electrode, E_0 is the standard potential of the RM redox couple, R is the universal gas constant, T is the temperature, z is the electron number of the redox reaction, F is the Faraday constant and $c^{ss}_{RM^+}(0)$, $c^{ss}_{RM}(0)$ are the concentrations of RM^+, RM at the carbon surface. Using eqn (3), the Nernst equation transforms to the following expressions for the concentrations $c^{ss}_{RM^+}(0)$ and $c^{ss}_{RM}(0)$:

$$c^{ss}_{RM^+}(0) = c^0_{RM}\frac{\exp(\Theta)}{1+\exp(\Theta)} \quad (7)$$

$$c^{ss}_{RM}(0) = c^0_{RM}\frac{1}{1+\exp(\Theta)} \quad (8)$$

$$\text{with: } \Theta = \frac{zF(E-E_0)}{RT}, \quad (9)$$

whereas Θ corresponds to the exponents of eqn (7) and (8). Since both species are assumed to exhibit equal diffusion coefficients, constant concentration gradients are obtained under steady state conditions. Hence, the concentrations of RM and RM^+ within the electrolyte are directly determined by the surface concentrations, compare eqn (4), (7) and (5), (8). Fig. 3 shows the concentration profiles at different potentials of the carbon electrode for the redox couple $TEMPO^+$/TEMPO. Herein, the total amount of $TEMPO^+$, resp. RM^+, raises with increasing electrode potential E.

Diffusion

• To describe charge transport along the distance d, Fick's 1st law is adapted to the model conditions:

$$j^{ss} = zFD\frac{c^{ss}_{RM}(d) - c^{ss}_{RM}(0)}{d}, \quad (10)$$

where j^{ss} is the current density under stationary conditions. Since the concentration gradients are similar for RM and RM^+, the choice of the investigated species is arbitrary. According to eqn (5) and (8), the following expressions are finally obtained for potentiostatic and galvanostatic experiments:

$$j^{ss} = \frac{zFc^0_{RM}D}{d}\frac{\exp(\Theta)}{1+\exp(\Theta)} \quad (11)$$

$$E = E_0 + \frac{RT}{zF}\ln\left(\frac{j^{ss}d}{zFc^0_{RM}D - j^{ss}d}\right) \quad (12)$$

A related set of expressions was proposed by Narayanan *et al.* to describe the redox additive based overcharge protection in lithium ion batteries.[26] Both equations indicate that the charging of Li–O_2 cells with redox mediators is determined by several independent parameters. Of particular interest are the parameters E_0 and D, which are related to the chemical structure of the redox mediator. Herein, the redox potential E_0 has a distinctly higher impact on the charging profiles than the diffusion coefficient D. The parameter d describes the lengths of the RM/RM^+ diffusion paths, which is surmised to change during the charging step and which strongly depend on the microstructure of the carbon electrode and the discharge product. This step in the over-all kinetics will be further discussed on the basis of experimental data, see Section 4.2.

4. Results and discussion

4.1 Experimental validation of the electrochemical model

Regular Li–O_2 cells are not suitable for validating the presented model, since the distance between Li_2O_2 and the uncovered parts of the electrode surface is inhomogeneous and not well specified. Hence, we also developed a modified cell setup denoted as cell 1, which provides well defined values of c^0, d and E. The setup was comprised of a glassy carbon working electrode, a LFP counter electrode and a lithium reference electrode, compare Fig. 1. A porous separator was placed between the electrodes hosting a liquid electrolyte with different concentrations of TEMPO, compare Fig. S1a (ESI†). Herein, LFP served as redox substitute for Li_2O_2, since $TEMPO^+$ is directly reduced at the LFP surface (E_0 = 3.45 V *vs.* Li^+/Li). In order to validate the presented model, c^0, d and E were successively varied and the corresponding shuttle current was determined under potentiostatic conditions.

Fig. 4a exemplarily shows the current profiles for different initial TEMPO concentrations c^0 at fixed values of E and d. After applying a potential of 3.95 V *vs.* Li^+/Li at the time t = 0 min, all current profiles directly increase, subsequently decrease and finally exhibit a shallow plateau. The current plateau is attributed to the shuttle current j^{ss} under steady state conditions, which was described by the presented model. Stationary conditions were obtained after about 3 min, which is consistent with the expected time of $d^2/D \approx 3$ min using d = 200 μm and $D = 2.4 \times 10^{-6}$ cm^2 s^{-1}, compare Table 1. During the pre-stationary period, TEMPO was oxidized at the carbon electrode and LFP itself was predominantly reduced by inserting lithium, which caused a successive increase of the total $TEMPO^+$ concentration. The stationary shuttle currents j^{ss} of the different TEMPO concentrations are illustrated in Fig. 4b. To compare the experimental data with the predictions of the electrochemical model, the shuttle current was calculated for the complete concentration range by using eqn (11) with z = 1, T = 298 K and the parameters of Table 1. Since the diffusion processes are significantly affected by the porous separator, the diffusion

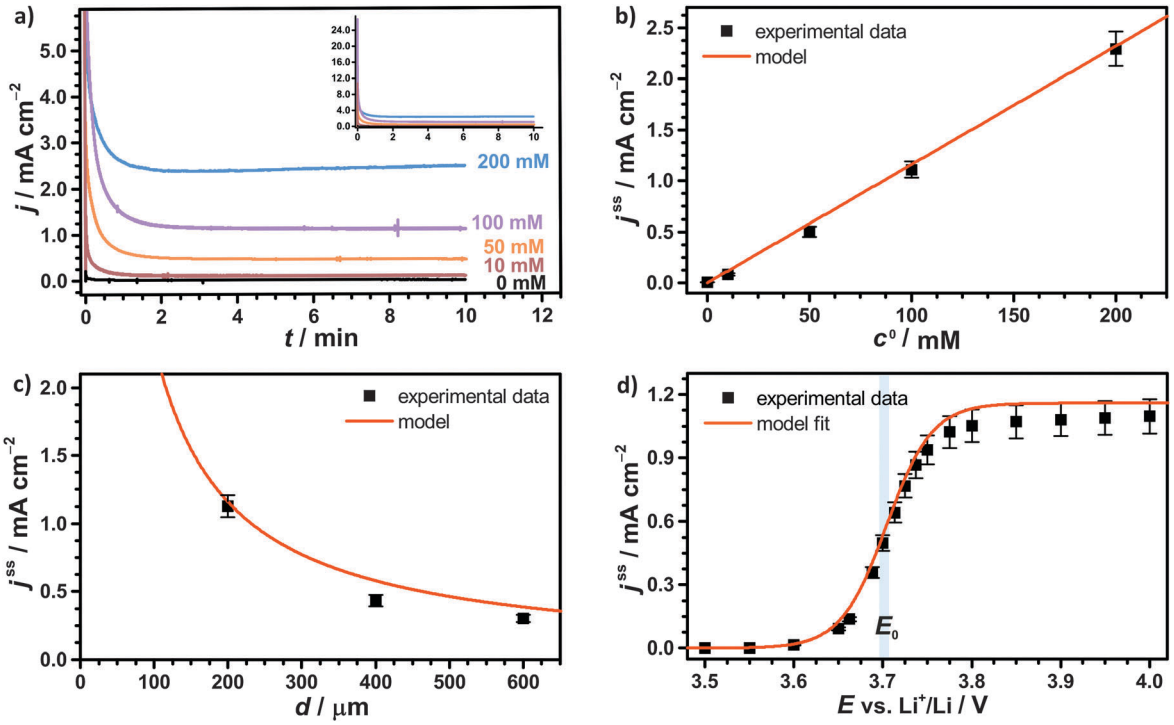

Fig. 4 Potentiostatic measurements of 1 M LiTFSI/diglyme with various TEMPO concentration using a GC working electrode, a LFP counter electrode and a lithium reference electrode, compare Fig. 1; (a) current–time profiles for different TEMPO concentrations c^0 using E = 3.95 V *vs.* Li$^+$/Li and d = 200 µm; (b) stationary shuttle current j^{ss} at different c^0, derived from the final data points of (a); (c) stationary shuttle current j^{ss} at different d, obtained at c^0 = 100 mM and E = 3.95 V *vs.* Li$^+$/Li, and (d) stationary shuttle current j^{ss} at different E, obtained at c^0 = 100 mM and d = 200 µm; the original current–time profiles of (c) and (d) are illustrated in Fig. S2a and b (ESI†).

Table 1 Parameters for the electrochemical model (according to eqn (11))

ε^a/%	$E^{0\,b}$ *vs.* Li$^+$/Li/V	$D^c/10^{-6}$ cm^2 s^{-1}	$D_{eff}{}^d/10^{-6}$ cm^2 s^{-1}
87 (±4)	3.70 (±0.01)	3.9 (±0.4)	2.4 (±0.4)

[a] See Section 2.2.2. [b] E_0 was determined by CV using the setup of the potentiostatic measurements with c^0(TEMPO) = 100 mM, comp. Fig. S1b (ESI). [c] D was derived from CV measurements using a glass cell with 10 mM TEMPO, see Fig. S3a (ESI) and Table 2. [d] D_{eff} was derived from D using eqn (13) and α = 3.44.[29]

coefficient of TEMPO was adapted to the experimental conditions by using the following equation:

$$D_{eff} = D \cdot \frac{\varepsilon}{\tau}, \quad \text{with } \tau = \varepsilon^{1-\alpha} \tag{13}$$

Herein, D is the diffusion coefficient of TEMPO in the bulk electrolyte, ε is the porosity of the separator and τ is the corresponding tortuosity, which is expressed by the Bruggemann correlation.[28]

The shuttle currents j^{ss} at stationary conditions are in good agreement with the experimental results at different concentrations, as illustrated in Fig. 4b. Herein, the simulated profile almost matches all data within the experimental errors validating the electrochemical model and the applied parameters. Additionally, the stationary shuttle currents j^{ss} were determined for different distances d of the diffusion paths (Fig. 4c), which were obtained by changing the interelectrode distance d. The experimental results and the simulated profile agree qualitatively, showing a hyperbolic decrease of the shuttle currents with increasing distance. At large distances however, the experimental results dropped below the predicted values of the model. These findings were mainly ascribed to an insufficient contact between the different layers of separator, which were used to increase the interelectrode gap. We want to point out that the presented investigations serve as model experiments to study the influence of the diffusion distance on the shuttle current, while the absolute length of the diffusion paths in Li–O_2 batteries is surmised to be significantly smaller (<1 µm) than the applied distances.

Finally, the potential E of the carbon electrode was varied under otherwise fixed conditions and the corresponding shuttle currents were determined, see Fig. 4d. The experimental results are consistent with the simulated profile representing the logarithmic relation between j^{ss} and E of eqn (11). The stationary shuttle j^{ss} increases steeply within a small potential range of approx. $E_0 \pm 150$ mV, which defines the main working range of the redox mediator. At $E < (E_0 - 150\text{ mV})$, the redox mediator is marginally oxidized and the charge transport succumbs. At $E > (E_0 + 150\text{ mV})$, the maximal transport rate is already obtained and a further increase of E will not lead to considerable higher stationary shuttle currents j^{ss}. We note that the agreement between model and experiment justifies the initial assumptions, in particular the assumption of negligible charge transfer resistances.

4.2 Combining molecular structure and electrochemical properties: nitroxides in the context of Li–O_2 batteries

As expected and well described by the presented model, the chemical structure of the redox mediator has a significant impact on the charging profile in terms of E_0 and D. Under practical conditions the stability resp. chemical reversibility of the redox couple has to be additionally considered, since degradation reactions are a serious problem in Li–O_2 batteries. Extending our previous study with TEMPO,[19] these effects will be studied in the following for the chemical group of nitroxides.

Nitroxides are stable radicals and undergo versatile redox reactions that are the basis of numerous applications in organic chemistry, polymer chemistry, and biology. Scheme 1 illustrates the typical oxidation and reduction reactions of nitroxides **1** in an aprotic solvent,[30–32] which have been studied extensively by electron paramagnetic resonance (EPR).[33–35] The oxidation to the corresponding oxoammonium cation **2** was shown to be highly reversible in case of different cyclic nitroxides such as nitroxides with a piperidine or adamantane backbone.[36–38] The redox couple oxoammonium cation/nitroxide with potentials $E > 3.5$ V *vs.* Li^+/Li provides the basis of the catalytic oxidation of Li_2O_2 in Li–O_2 cells.[19,39] At potentials $E \ll 3.0$ V *vs.* Li^+/Li nitroxides are reduced to the corresponding aminoxy anion **3**,[35,40,41] which was reported to be an irreversible process.[19,37]

To derive a relation between the chemical structure and the corresponding charging profile we investigated typical representatives of different nitroxide subgroups. The corresponding compounds are illustrated in Scheme 2 comprising the classical piperidine-based nitroxides TEMPO **4** and 4-methoxy-TEMPO **5**, the azaadamanatane-based nitroxides AZADO **6** and 1-Me-AZADO **7**, the azaphenalene-based nitroxide TMAO **8** and the two acyclic nitroxides 2,2,5-trimethyl-4-phenyl-3-azahexane-3-nitroxide **9** and *tert*-amyl-*tert*-butyl nitroxide **10**.

4.2.1 Cyclic voltammetry. The electrochemical behaviour of the different nitroxides in diglyme was characterized by cyclic voltammetry, (*cf.* Fig. 5a and b). All cyclic nitroxides show a reversible oxidation to an oxoammonium cation **2** at voltages >3.5 V *vs.* Li^+/Li and an irreversible reduction to the lithiated aminoxy anion **3**, which is in accordance with aforementioned studies in acetonitrile.[38,42,43]

In contrast, an electrochemically irreversible oxidation is observed for both acyclic nitroxides excluding the use as redox mediators in Li–O_2 batteries. This is in line with several studies on the electrochemistry of the related compound di-*tert*-butyl nitroxide (DTBN) in acetonitrile.[36,44,45] However, Bogart *et al.* have recently reported about reversible oxoammonium/nitroxide redox couples in case of several acyclic 2-pyridylhydroxylamines.[46] Based on these findings, the introduction of pyridiyl substituents in α-position to the NO moiety might be a promising strategy to convert the investigated acyclic nitroxides into stable redox mediators for Li–O_2 batteries.

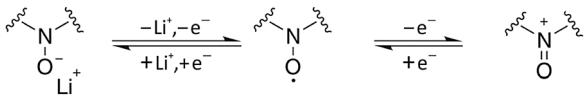

3 **1** **2**

Scheme 1 Oxidation and reduction reactions of nitroxides in aprotic electrolytes.

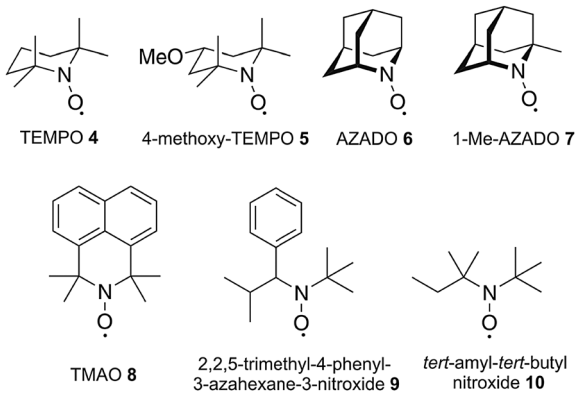

Scheme 2 Chemical structures of the investigated nitroxides.

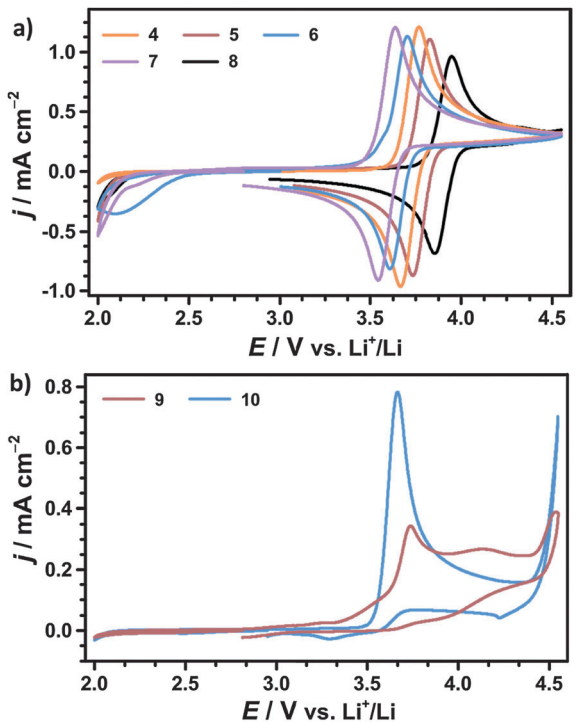

Fig. 5 (a) Cyclic voltammograms (CVs) of 10 mM TEMPO **4**, 10 mM 4-methoxy-TEMPO **5**, 10 mM AZADO **6**, 10 mM 1-Me-AZADO **7**, 10 mM TMAO **8** and (b) 10 mM 2,2,5-trimethyl-4-phenyl-3-azahexane-3-nitroxide **9**, 10 mM *tert*-amyl-*tert*-butyl nitroxide **10** in 1 M LiTFSI/diglyme with a scan speed of 50 mV s^{-1}; CVs obtained in a bulk electrolysis cell according to 2.3 under argon atmosphere (p = 1 bar).

To further characterize the cyclic nitroxides the redox potential E_0, the diffusion coefficient D and the ratio of cathodic and anodic peak currents $j_{p,c}/j_{p,a}$ were determined by CV, compare Table 2. Assuming equal diffusion coefficients of the nitroxide and the oxoammonium cation, $j_{p,c}/j_{p,a}$ is considered as an indicator for the chemical reversibility of the redox reaction.[47] A fully reversible redox reaction is characterized by a ratio of

Table 2 Electrochemical properties of the oxoammonium cation/nitroxide redox couples

Nitroxide	$E^{0\,a}$ *vs.* Li^+/Li/V	$j_{p,c}/j_{p,a}$	$D^b/10^{-6}$ cm^2 s^{-1}
4	3.73 (±0.01)	0.99 (±0.01)	3.9 (±0.4)
5	3.76 (±0.02)	0.97 (±0.01)	3.3 (±0.3)
6	3.65 (±0.01)	0.90 (±0.02)	3.3 (±0.3)
7	3.60 (±0.01)	0.92 (±0.03)	3.9 (±0.3)
8	3.89 (±0.01)	0.92 (±0.02)	2.5 (±0.4)

^{a} $E^0 = (E_{p,c} + E_{p,a})/2$. ^{b} D: diffusion coefficient of the uncharged nitroxide based on Randles–Sevcik equation, compare eqn (14).

exactly 1.00, whereas values significantly below 1.00 indicate a loss of oxoammonium cations by consecutive degradation reactions.

We infer that TEMPO and 4-methoxy-TEMPO provide the most stable oxoammonium cations with $j_{p,c}/j_{p,a}$ values of nearly 1.00. The oxoammonium cations of AZADO and 1-Me-AZADO show significantly lower stabilities. This is mainly caused by a reduced steric protection of the NO moiety due to one resp. two H atoms in the α-position. The oxidation of TMAO is likewise less reversible, which is probably caused by the unfavourable conformation of the oxoammonium cation due to the sp^2 carbon atoms in vicinity to the NO moiety.[22]

The redox potentials E_0 of the investigated nitroxides range from 3.60 to 3.89 V *vs.* Li^+/Li indicating that E_0 is mainly determined by the redox active NO moiety. The chemical substituents further refine the redox potential E_0 within a range of approx. 300 mV, which will be further discussed below. 4-Methoxy-TEMPO provides a slightly higher E_0 than TEMPO which is attributed to the electron-withdrawing inductive ($-I$) effect of the methoxy group. An even higher E_0 is determined for TMAO fitting well with CV experiments in acetonitrile.[43] However, computational studies predicted a significantly lower redox potential of TMAO by assuming mesomeric stabilisation of the oxoammonium cation by the aromatic backbone. Since we observe a drastically deviating result in our experiments, the mesomeric stabilisation across the six-membered ring seems to be of minor influence compared to the $-I$ effect of the sp^2 carbons.[43,48] AZADO and 1-Me-AZADO show significantly lower redox potentials than TEMPO, which matches well with previous studies in acetonitrile.[38,49] We assume that the low redox potentials are mainly attributed to the rigid structure of the adamantane skeleton, which fixes three C–C bonds in a parallel orientation to the π bond of the NO moiety. Hence, the oxoammonium cations of AZADO or 1-Me-AZADO are stabilised by hyperconjugation, while more flexible molecules like TEMPO facilitate hyperconjugation solely in transient conformations.

The diffusion coefficients D of the nitroxides were determined from the CV data using the Randles–Sevcik equation,[47] which describes the relation between the anodic peak current $j_{p,a}$ and the scan rate v:

$$j_{p,a} = 0.4463zFc^0\left(\frac{zFvD}{RT}\right)^{\frac{1}{2}} \quad (14)$$

Here, z the number of transferred electrons, F the Farraday constant, c^0 the initial concentration of the nitroxides, R the universal gas constant and T the temperature. Fig. 6 illustrates the CVs of 1-Me-AZADO at different scan rates under argon atmosphere. The CVs show a clear diffusion control in the investigated scan rate range due to a nearly constant separation between cathodic and anodic peak current ΔE_{pp}. The data of the other nitroxides are shown in the ESI,† compare Fig. S3 (ESI†). The diffusion coefficients preponderantly correlate with the reciprocal size of the nitroxides, which is in line with the Stokes-Einstein equations: $D_{TEMPO} \approx D_{1\text{-Me-AZADO}} > D_{AZADO} \approx D_{4\text{-methoxy-TEMPO}} \gg D_{TMAO}$. Solely the relation $D_{1\text{-Me-AZADO}} > D_{AZADO}$ does not comply with the reciprocal molecular sizes, since 1-Me-AZADO exhibits an additional methyl group compared to AZADO. These findings might be attributed to unequal solvation of both molecules within the electrolyte. The diffusion coefficients distinctly depend on the solvent and the salt concentration, as indicated by a comparison with previous studies: while we determined the diffusion coefficient of TEMPO to be 3.9×10^{-6} cm^2 s^{-1} in 1 M LiTFSI/diglyme, previous studies reported values of approx. 1.4×10^{-5} cm^2 s^{-1} in 0.1 M LiTFSI/diglyme or 3.6×10^{-6} cm^2 s^{-1} in 1 M $LiPF_6$/(EC/DEC).[19,50]

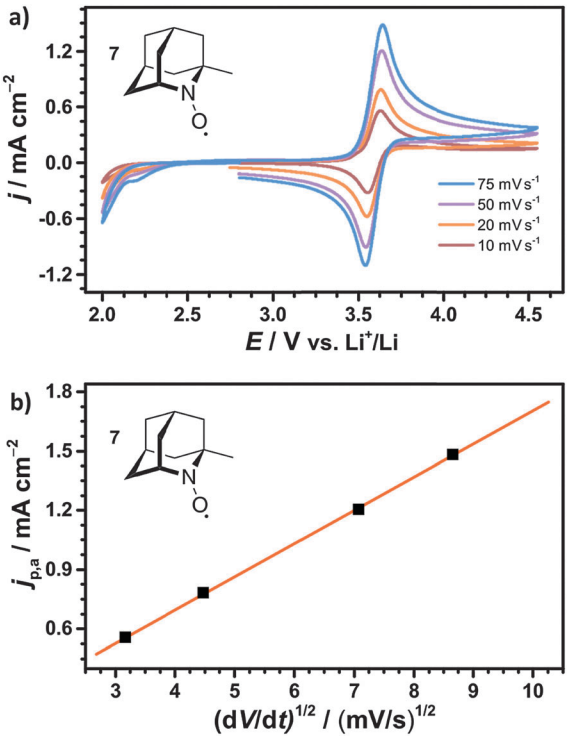

Fig. 6 (a) Cyclic voltammograms (CVs) of 10 mM 1-Me-AZADO **7** in 1 M LiTFSI/diglyme at different scan speeds and (b) the corresponding Randles–Sevcik plot of the anodic peak currents $j_{p,a}$; the linear fit is given by $y = 0.030 + 0.167x$. All CVs were obtained in a bulk electrolysis cell according to 2.3 under argon atmosphere (p = 1 bar).

The investigated cyclic nitroxides also showed reversible oxidation under oxygen atmosphere as exemplarily illustrated for 1-Me-AZADO in Fig. 7a. Since the reduction peaks in argon and oxygen atmosphere were identical for all nitroxides, oxygen is considered to have no significant influence on the stability of the oxoammonium cations within the investigated range of scan

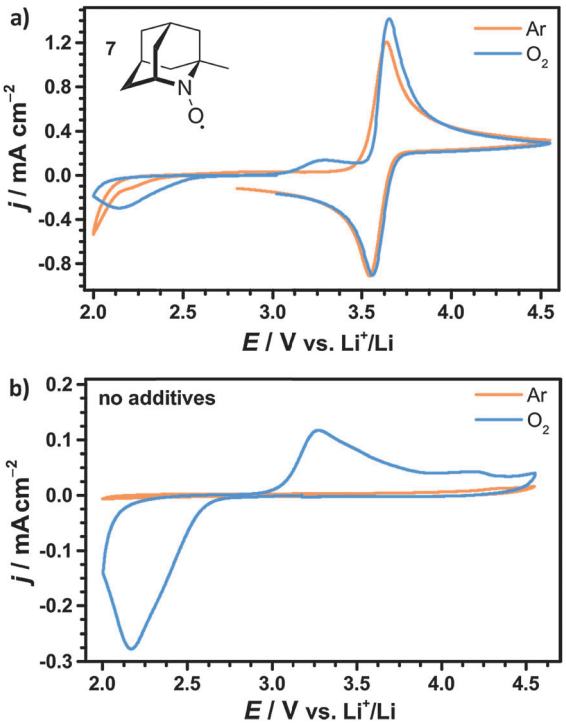

Fig. 7 Cyclic voltammograms (CVs) of 1 M LiTFSI/diglyme (a) with 10 mM 1-Me-AZADO **7** or (b) without additives under argon and oxygen atmospheres (p = 1 bar). The CVs were obtained in a bulk electrolysis cell according to 2.3 with a scan speed of 50 mV s^{-1}.

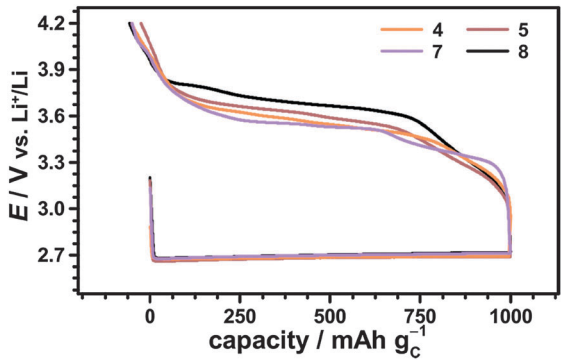

Fig. 8 First cycle of Li–O_2 cells with 10 mM TEMPO **4**, 4-methoxy-TEMPO **5**, 10 mM 1-Me-AZADO **7** and 10 mM TMAO **8** in 1 M LiTFSI/diglyme using a fixed discharge capacity of 1000 mA h g_C^{-1}, j = 0.1 mA cm^{-2} and $p(O_2)$ = 1 bar.

rates. Two additional peaks arose in the presence of oxygen including the ORR at 2.1 V *vs.* Li$^+$/Li and the OER at 3.3 V *vs.* Li$^+$/Li. Both peaks were similar to the peaks in the CV of the pure electrolyte without nitroxides, see Fig. 7b. The oxidation peak of 1-Me-AZADO increased in the presence of oxygen indicating a direct reduction of the oxoammonium cation at the electrode surface by residual Li_2O_2. This catalytic effect is less pronounced for the nitroxides with higher redox potentials since the amount of Li_2O_2 was electrochemically reduced before the oxidation peak of the nitroxide was reached, see Fig. S4 (ESI†).

4.2.2 Galvanostatic cycling of Li–O_2 cells. The most stable nitroxides TEMPO, 4-methoxy-TEMPO, 1-Me-AZADO and TMAO were subsequently studied under typical cycling conditions of a Li–O_2 cell. Herein, a classical setup was chosen comprising of a porous carbon cathode, a lithium anode and lithium reference electrode. Further details of this electrochemical cell, denoted as "cell 2", are listed in Section 2.4.1 and Fig. 2. The first cycle of the Li–O_2 cells is illustrated in Fig. 8 using a fixed discharge capacity of 1000 mA h g_C^{-1}. It is clearly evident that the four nitroxides show mutually different charging plateaus correlating rather to the order of the redox potentials E_0 than to the diffusion coefficients D. These findings agree with the presented model, since E_0 has a stronger impact on the charging potential than D according to eqn (12). All nitroxides significantly reduced the charging overpotentials compared to a Li–O_2 without additives under otherwise similar conditions, see Fig. S5a (ESI†).

Herein, the Li–O_2 cell with 1-Me-AZADO provided the lowest charging potentials emphasizing the promising role of nitroxides with an adamantane skeleton. Further reduction of the charging potential is expected for using the non-commercial nitroxide 1,3 Dime-AZADO, which showed the lowest redox potential in a broad screening of nitroxides by Shibuya *et al.*[38] Due to increased steric protection of the NO moiety we expected that 1,3 Dime-AZADO will additionally provide an oxoammonium cation of higher stability than AZADO or 1-Me-AZADO.

The charging potentials were not fixed at a certain value but showed a continuously increasing profile. Herein, charging voltages from about −200 mV to ±0 mV *vs.* E_0 appeared, while the potentiostatic measurements provided an active range from ≈−150 mV to ≈±150 mV *vs.* E_0. We assume that the short diffusion distances d at the beginning of the charging step facilitated an adequate shuttle current already at ≈−200 mV *vs.* E_0 complying with the applied current density. During charging, Li_2O_2 depletes in the direct vicinity of the uncovered surface areas which is expected to continuously raise d. Hence, the cathodic potential simultaneously increased to provide a constant j for the whole charging step, compare eqn (12).

The catalytic effects of the different nitroxides were not limited to the fixed discharge capacity of 1000 mA h g_C^{-1}, but were also observed in case of fully discharged Li–O_2 cells. Fig. 9 shows the first cycle of Li–O_2 cells with and without 1-Me-AZADO using a fixed cut-off voltage of 2.0 V. The corresponding cycling profiles of Li–O_2 cells with TEMPO, 4-methoxy-TEMPO and TMAO are shown in the Fig. S6 (ESI†). Herein, all Li–O_2 cells with nitroxides exhibited significantly lower charging potentials than the cell without additives, fitting well to the cycling measurements restricted by a fixed discharge capacity of 1000 mA h g_C^{-1} (Fig. 8). 1-Me-AZADO, for instance, reduced the charging overvoltages by 200 to 400 mV depending on the depth of charge (DOC), see Fig. 9. The discharge capacity of Li–O_2 cells with nitroxides ranged from 3500 mA h g_C^{-1} in case of TEMPO and 4-methoxy-TEMPO to ≈5000 mA h g_C^{-1} in case of 1-Me-AZADO. Under similar conditions, the Li–O_2 cell without additives provided a capacity of ≈5000 mA h g_C^{-1}. These findings indicate that at least some of the investigated nitroxides directly affect the discharge processes, which is in line with a previous study on TEMPO in Li–O_2 batteries.[19]

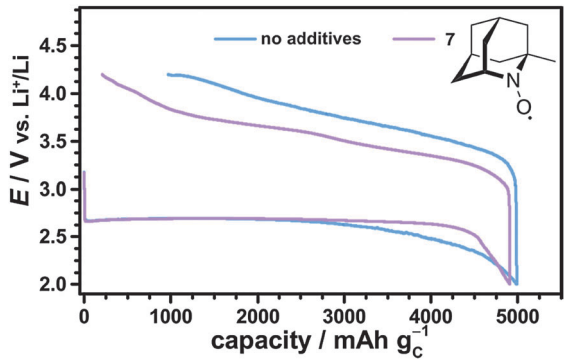

Fig. 9 First cycle of Li–O_2 cells with 1 M LiTFSI/diglyme containing either 10 mM 1-Me-AZADO **7** or no additive; the cells were discharged to a cut-off potential of 2.0 V and subsequently charged to 4.2 V using j = 0.1 mA cm^{-2} and $p(O_2)$ = 1 bar.

According to eqn (12), reduced charging potentials are likewise expected in case of higher redox mediator concentrations c^0. Indeed, the charging overpotentials in Li–O_2 cells further decreased by 100 mV on average as the TEMPO concentration of the electrolyte was increased from 10 mM to 100 mM, see Fig. S7 (ESI†). Compared to E_0, the impact of c^0 on the charging potential E is less pronounced representing the different sensitivities of E to E_0 and c^0 in eqn (12). The Li–O_2 cell with 100 mM TEMPO additionally exhibited a significant overcharge, which is probably attributed to the oxidation of TEMPO molecules in the bulk electrolyte during the last charging period. However, these processes are beyond the scope of this electrochemical study and will be investigated separately.

The formation and decomposition of Li_2O_2 during cycling was investigated by X-ray diffraction (XRD) analysis of the carbon electrode after discharge and charge. For this purpose Li–O_2 cells were fully discharged and subsequently charged to 4.2 V *vs.* Li$^+$/Li, which was reported to be insufficient to fully oxidize Li_2O_2 without additional catalysts.[19] The corresponding diffraction patterns are exemplarily shown for the use of 1-Me-AZADO in Fig. 10, the data of the residual nitroxides are shown in Fig. S8 (ESI†). In case of all nitroxides only Li_2O_2 was formed as crystalline reaction product after discharge to 2.0 V. However, non-crystalline degradation products like lithium carbonate, lithium acetate or lithium formate are expected to be simultaneously formed in minor fractions, as already shown for regular Li–O_2 cells as well as for cells with TEMPO.[5,19,21] After charging the Li–O_2 cells to 4.2 V, Li_2O_2 was fully decomposed in all Li–O_2 cells with nitroxides since the corresponding diffraction patterns disappeared completely. These findings provide evidence that the charging plateau directly corresponds to the catalytic oxidation of Li_2O_2 by the oxoammonium cation/nitroxide redox couple. In a previous study it was additionally shown that the charging plateau in Li–O_2 cells with TEMPO is exclusively accompanied by the evolution of oxygen at voltages below 4.0 V, while CO_2 formation was solely detected above 4.0 V.[19]

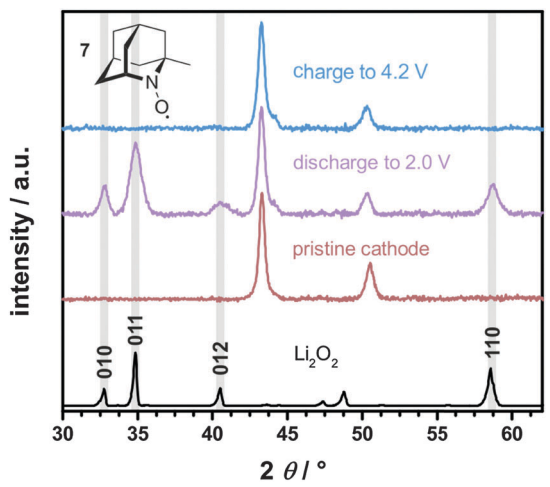

Fig. 10 XRD patterns of the carbon electrode after discharge and charge in a Li–O_2 cell with 10 mM 1-Me-AZADO **7** in 1 M LiTFSI/diglyme, j = 0.1 mA cm^{-2} and $p(O_2)$ = 1 bar; the cycling profile is illustrated in Fig. 9. Li_2O_2 diffraction pattern matches the typical Li_2O_2 faces (ICSD 98-018-0557).

5. Conclusion

Dissolved redox mediators, like nitroxides, lead to a distinct reduction of the charging overvoltages in Li–O_2 batteries. We systematically studied the charging of Li–O_2 cells with redox mediators and derived an electrochemical model for charge transfer under steady state conditions. The model was confirmed by potentiostatic experiments, which used a flat LFP electrode as an appropriate redox substitute for Li_2O_2. Based on the presented model the crucial impact factors for the charging processes were identified. These include external cycling settings, the distances of the diffusion paths to the Li_2O_2 particles and (electro)chemical properties of the redox mediator system. We applied the model to several cyclic nitroxides, which exhibit reversible oxidations reactions under the conditions of Li–O_2 batteries. Herein, we directly correlated the chemical structures of the nitroxide to their redox potentials, which mainly determined the charging potentials of the corresponding Li–O_2 cells. Among the selected nitroxides, 1-Me-AZADO was the most efficient redox mediator providing charging potentials below 3.6 V *vs.* Li$^+$/Li. The results of this work are not limited to nitroxides, but will also contribute to the optimization of other redox active compounds and support the further development of Li–O_2 batteries with redox mediators.

Acknowledgements

This project was supported by the BASF International Network for Batteries and Electrochemistry. B. J. Bergner was supported by a Kekulé studentship of the Funds of the Chemical Industry (FCI, Frankfurt, Germany). The authors thank Dr B. Luerßen (Justus-Liebig University Giessen) and Dr A. Garsuch (BASF SE) for fruitful discussions. We gratefully acknowledge B. Westphal (Technical University Braunschweig) for providing LFP electrodes, A. Seitz (Justus-Liebig University Giessen) for synthesizing TMAO, and M. von der Lehr (Justus-Liebig University Giessen) for mercury intrusion porosimetry measurements.

References

1 A. C. Luntz and B. D. McCloskey, *Chem. Rev.*, 2014, **114**, 11721–11750.
2 R. Black, S. H. Oh, J. Lee, T. Yim, B. Adams and L. F. Nazar, *J. Am. Chem. Soc.*, 2012, **134**, 2902–2905.
3 V. Viswanathan, K. S. Thygesen, J. S. Hummelshøj, J. K. Nørskov, G. Girishkumar, B. D. McCloskey and A. C. Luntz, *J. Chem. Phys.*, 2011, **135**, 214704.
4 C. Xia, M. Waletzko, L. Chen, K. Peppler, P. J. Klar and J. Janek, *ACS Appl. Mater. Interfaces*, 2014, **6**, 12083–12092.
5 S. A. Freunberger, Y. Chen, N. E. Drewett, L. J. Hardwick, F. Bardé and P. G. Bruce, *Angew. Chem., Int. Ed.*, 2011, **50**, 8609–8613.
6 B. D. McCloskey, A. Speidel, R. Scheffler, D. C. Miller, V. Viswanathan, J. S. Hummelshøj, J. K. Nørskov and A. C. Luntz, *J. Phys. Chem. Lett.*, 2012, **3**, 997–1001.
7 R. Padbury and X. Zhang, *J. Power Sources*, 2011, **196**, 4436–4444.
8 Y. C. Lu and Y. Shao-Horn, *J. Phys. Chem. Lett.*, 2013, **4**, 93–99.
9 P. Hartmann, C. L. Bender, M. Vračar, A. K. Dürr, A. Garsuch, J. Janek and P. Adelhelm, *Nat. Mater.*, 2013, **12**, 228–232.
10 P. Hartmann, D. Grübl, H. Sommer, J. Janek, W. G. Bessler and P. Adelhelm, *J. Phys. Chem. C*, 2014, **118**, 1461–1471.
11 Y. Hase, T. Shiga, M. Nakano, K. Takechi and N. Setoyama, *US Pat.*, Appl. No. 20090239113, 2009.
12 G. V. Chase, S. Zecevic, W. Walker, J. Uddin, K. A. Sasaki, V. Giordani, V. Bryantsev, M. Blanco and D. D. Addison, *US Pat.*, Appl. No. 20120028137, 2012.
13 Y. Chen, S. A. Freunberger, Z. Peng, O. Fontaine and P. G. Bruce, *Nat. Chem.*, 2013, **5**, 489–494.
14 W.-J. Kwak, D. Hirshberg, D. Sharon, H.-J. Shin, M. Afri, J.-B. Park, A. Garsuch, F. F. Chesneau, A. A. Frimer, D. Aurbach and Y.-K. Sun, *J. Mater. Chem. A*, 2015, **3**, 8855–8864.
15 D. Sharon, D. Hirsberg, M. Afri, F. Chesneau, R. Lavi, A. A. Frimer, Y.-K. Sun and D. Aurbach, *ACS Appl. Mater. Interfaces*, 2015, **7**, 16590–16600.
16 D. Sun, Y. Shen, W. Zhang, L. Yu, Z. Yi, W. Yin, D. Wang, Y. Huang, J. Wang, D. Wang and J. B. Goodenough, *J. Am. Chem. Soc.*, 2014, **136**, 8941–8946.
17 S. Matsuda, S. Mori, K. Hashimoto and S. Nakanishi, *J. Phys. Chem. C*, 2014, **118**, 28435–28439.
18 S. Matsuda, S. Mori, Y. Kubo, K. Uosaki, K. Hashimoto and S. Nakanishi, *Chem. Phys. Lett.*, 2015, **620**, 78–81.
19 B. J. Bergner, A. Schürmann, K. Peppler, A. Garsuch and J. Janek, *J. Am. Chem. Soc.*, 2014, **136**, 15054–15064.
20 H.-D. Lim, H. Song, J. Kim, H. Gwon, Y. Bae, K.-Y. Park, J. Hong, H. Kim, T. Kim, Y. H. Kim, X. Lepró, R. Ovalle-Robles, R. H. Baughman and K. Kang, *Angew. Chem., Int. Ed.*, 2014, **53**, 4007–4012.
21 M. M. Ottakam Thotiyl, S. A. Freunberger, Z. Peng and P. G. Bruce, *J. Am. Chem. Soc.*, 2013, **135**, 494–500.
22 J. P. Blinco, J. C. McMurtrie and S. E. Bottle, *Eur. J. Org. Chem.*, 2007, 4638–4641.
23 R. G. Compton and C. E. Banks, *Understanding voltammetry*, Imperial College Press, 2nd edn, 2011.
24 E. L. Cussler, *Diffusion Mass Transfer in Fluid Systems*, Cambridge University Press, 3rd edn, 2007.
25 K. M. Abraham, *J. Electrochem. Soc.*, 1990, **137**, 1856–1857.
26 S. R. Narayanan, S. Surampudi, A. I. Attia and C. P. Bankston, *J. Electrochem. Soc.*, 1991, **138**, 2224–2229.
27 B. D. Adams, C. Radtke, R. Black, M. L. Trudeau, K. Zaghib and L. F. Nazar, *Energy Environ. Sci.*, 2013, **6**, 1772–1778.
28 D. A. G. Bruggeman, *Ann. Phys.*, 1935, **24**, 636–664.
29 A. Nyman, M. Behm and G. Lindbergh, *Electrochim. Acta*, 2008, **53**, 6356–6365.
30 C. J. Hawker, *J. Am. Chem. Soc.*, 1994, **116**, 11185–11186.
31 M. C. Krishna, D. A. Grahame, A. Samuni, J. B. Mitchell and A. Russo, *Proc. Natl. Acad. Sci. U. S. A.*, 1992, **89**, 5537–5541.
32 P. L. Anelli, C. Biffi, F. Montanari and S. Quici, *J. Org. Chem.*, 1987, **52**, 2559–2562.
33 A. Samuni, A. J. Carmichael, A. Russo, J. B. Mitchell and P. Riesz, *Proc. Natl. Acad. Sci. U. S. A.*, 1986, **83**, 7593–7597.
34 S. Morris, G. Sosnovsky, B. Hui, C. O. Huber, N. U. M. Rao and H. M. Swartz, *J. Am. Pharm. Assoc.*, 1991, **80**, 149–152.
35 J. R. Fish, S. G. Swarts, M. D. Sevilla and T. Malinski, *J. Phys. Chem.*, 1988, **92**, 3745–3751.
36 M. Tsunaga, C. Iwakura and H. Tamura, *Electrochim. Acta*, 1973, **18**, 241–245.
37 T. Yamasaki, F. Mito, Y. Ito, S. Pandian, Y. Kinoshita, K. Nakano, R. Murugesan, K. Sakai, H. Utsumi and K. Yamada, *J. Org. Chem.*, 2011, **76**, 435–440.
38 M. Shibuya, F. Pichierri, M. Tomizawa, S. Nagasawa, I. Suzuki and Y. Iwabuchi, *Tetrahedron Lett.*, 2012, **53**, 2070–2073.
39 Y. Hase, E. Ito, T. Shiga, F. Mizuno, H. Nishikoori, H. Iba and K. Takechi, *Chem. Commun.*, 2013, **49**, 8389–8391.
40 L. Tebben and A. Studer, *Angew. Chem., Int. Ed.*, 2011, **50**, 5034–5068.
41 T. Suga, K. Yoshimura and H. Nishide, *Macromol. Symp.*, 2006, **245–246**, 416–422.
42 S. D. Rychnovsky, R. Vaidyanathan, T. Beauchamp, R. Lin and P. J. Farmer, *J. Org. Chem.*, 1999, **64**, 6745–6749.
43 J. P. Blinco, J. L. Hodgson, B. J. Morrow, J. R. Walker, G. D. Will, M. L. Coote and S. E. Bottle, *J. Org. Chem.*, 2008, **73**, 6763–6771.
44 S. Kishioka and A. Yamada, *Electrochim. Acta*, 2005, **51**, 462–466.
45 L. McKay and R. J. LeSuer, *Electrochim. Acta*, 2008, **53**, 8305–8309.
46 J. A. Bogart, H. B. Lee, M. A. Boreen, M. Jun and E. J. Schelter, *J. Org. Chem.*, 2013, **78**, 6344–6349.
47 A. J. Bard and L. R. Faulkner, *Electrochemical Methods. Fundamentals and Applications*, John Wiley & Sons, 2nd edn, 2001.
48 J. L. Hodgson, M. Namazian, S. E. Bottle and M. L. Coote, *J. Phys. Chem. A*, 2007, **111**, 13595–13605.
49 M. Shibuya, M. Tomizawa, I. Suzuki and Y. Iwabuchi, *J. Am. Chem. Soc.*, 2006, **10**, 8412–8413.
50 M. Taggougui, B. Carré, P. Willmann and D. Lemordant, *J. Power Sources*, 2007, **174**, 643–647.